Journal of
Marine Science and Engineering

MDPI

Article

Relationship of the Quanta-to-Energy Ratio of Photosynthetically Active Radiation with Chlorophyll-*a* in Case I Seawater

Weibo Wang [1,2], Jianhua Zheng [3], Chunsheng Jing [1,2] and Jinping Zhao [4,*]

1 Ocean Dynamic Laboratory, Third Institute of Oceanography, Ministry of Natural Resources, Xiamen 361005, China
2 Fujian Provincial Key Laboratory of Marine Physical and Geological Processes, Xiamen 361005, China
3 Xiamen Institute of Environmental Science, Xiamen 361024, China
4 Key Laboratory of Physical Oceanography, Ministry of Education, Ocean University of China, Qingdao 266100, China
* Correspondence: jpzhao@ouc.edu.cn

Abstract: A predetermined quanta-to-energy ratio is often used in many ecosystem models to transform photosynthetically radiant flux density into photosynthetic photon flux density when light penetrates seawater. The calculation formula of the ratio is reduced in this study as the product of a constant and the defined principal wavelength. The principal wavelength is discussed in this paper and may be expressed as an exponential function using theoretical reasoning. The deviation of the principal wavelength is defined as the difference between two natural logarithms of the observed principal wavelength in real seawater and the simulated principal wavelengths of pure seawater under the same surface solar radiation. The deviation has a quasi-linear relationship with the non-water diffuse attenuation coefficient at 490 nm, which is related to the chlorophyll-*a* concentration. A semi-empirical formula between the deviation and chlorophyll-*a* concentration is established with a determination coefficient of more than 84%. In pure seawater, an empirical formula for the principal wavelength profile is also constructed. The parameterization formula for the quanta-to-energy ratio is provided as a function of the chlorophyll-*a* concentration and the surface principal wavelength. When applied to in situ observations, the statistical relative inaccuracy is found to be less than 10%. The parameterization formula can be applied to the ecosystem models to realize the transformation between photos and energy in the PAR waveband.

Keywords: photosynthetically active radiation; quanta-to-energy ratio; theoretical analysis; parameterization formula

check for updates

Citation: Wang, W.; Zheng, J.; Jing, C.; Zhao, J. Relationship of the Quanta-to-Energy Ratio of Photosynthetically Active Radiation with Chlorophyll-*a* in Case I Seawater. *J. Mar. Sci. Eng.* **2022**, *10*, 2005. https://doi.org/10.3390/jmse10122005

Academic Editor: Daniel M. Alongi

Received: 7 August 2022
Accepted: 12 December 2022
Published: 15 December 2022

Publisher's Note: MDPI stays neutral with regard to jurisdictional claims in published maps and institutional affiliations.

Copyright: © 2022 by the authors. Licensee MDPI, Basel, Switzerland. This article is an open access article distributed under the terms and conditions of the Creative Commons Attribution (CC BY) license (https://creativecommons.org/licenses/by/4.0/).

1. Introduction

The portion of solar energy used by the chloroplast of the plant for photosynthesis is known as photosynthetically active radiation (PAR) [1–3]. Its accurate quantification is required to predict gross primary production (GPP) [4–6], which is a key component of the global carbon cycle [5,7–9]. Photosynthetically active radiation is a broad phrase that encompasses both photon (Q) and energy (W) terms [1,2]. Photosynthetic photon flux density (Q) is defined as the number of photons incident per unit time on a unit surface in the 400–700 nm waveband (1 μmol m^{-2} s^{-1} = 6.022 × 10^{17} photons m^{-2} s^{-1}) [1,10].

The estimation of Q on the Earth's surface before the 1990s was difficult to accomplish due to a lack of sufficient satellite datasets [2,5]. Fortunately, there is a possible approach to convert to Q from solar radiation (R_s; W m^{-2}), which has been measured at regular intervals since the 1900s [5]. The technique has been used to convert Rs to Q in certain global ecosystem models (e.g., [9,11–13]). The conversion factor can be considered as a product of two ratios: (i) the fraction of the broadband energy flux that lies in the PAR waveband (400–700 nm), and (ii) the quanta-to-energy ratio of this band (Q/W) [14]. Researchers

have been studying the Q/Rs in different meteorological situations. It may have been followed since 1940 [15]. The impacts of the solar zenith angle (θ), dew point temperature, and clearness index have been studied in certain models [16–20]. Some researchers claim that the Q/Rs rise with θ (e. g., [19,21]), while others claim the contrary (e.g., [14,20]). Furthermore, according to other scientists, the association varies depending on the location or season (e.g., [18,22]). In particular, the Q/Rs changes within a range of 15% in response to seasonal and regional variations in atmospheric water vapor pressure [5,13]. Li, et al. [23] reported a quanta-to-energy ratio value of 4.57 μmol s^{-1} W^{-1}. The alterations in the quanta-to-energy ratio above the sea surface seen in several places are described by [24]. In a wide range of conditions, the ratio has a numerical value of 4.6 ± 1% μmol s^{-1} W^{-1} above the water surface. The quanta-to-energy ratio may change within 3% around McCree's constant value in response to changes in the solar zenith angle, dew point temperature, and clearness index. For most purposes, the use of McCree's value is probably acceptable above the water surface [13].

In the ocean, the quanta-to-energy ratio plays a major role in modulating Q/R_s, since most of the solar radiation that enters the ocean is concentrated between 400 and 700 nm [1]. However, few underwater studies on the quanta-to-energy ratio have been performed as a result of the lack of large-scale observation stations, such as the World Climate Research Program's Baseline Surface Radiation Network (WCRP-BSRN). In general, solar light entering seawater is rapidly reduced by the absorption and scattering impact of particles in the seawater within a few dozen of meters in the ocean [25,26]. Water molecules, phytoplankton, color-dissolved organic matter (CDOM), and detritus are the four primary types of particles that absorb sun energy [26,27]. Most infrared sun energy is absorbed by seawater molecules in a narrow layer under the surface. Ultraviolet radiation also transmits over a short distance due to the absorption of CDOM [27]. The deeper water can only be penetrated by visible light. As a result, the spectral distribution of solar radiation varies more in the water than in the atmosphere. Reinart, et al. [28] explore the profiles of the quanta-to-energy ratio for *Jerlov*'s oceanic and coastal water types, revealing that the ratio is regulated by the depth of the water body as well as its transparency. The quanta-to-energy ratio may differ by up to 24% from its value in the air [28]. In some models, however, a constant is still employed. In the simulation of developing ice algae, Lavoie, et al. [29] employ 4.56 μmol s^{-1} W^{-1}. The vertical profiles of the quanta-to-energy ratio are determined by the water types, and it decreases with depth for oceanic water types, whereas it increases with depth for turbid coastal water [28]. There will undoubtedly be substantial inaccuracies if only one constant is used.

The application of the quanta-to-energy ratio can address the incompatibility between the physical units in which PAR is often measured or reported, and the units that are appropriate for process-based modeling of photosynthesis [30]. Underwater biological processes and solar radiation simulations need to know how the quanta-to-energy ratio alters in the ocean. The profile of the quanta-to-energy ratio is closely related to the underwater attenuation material and identifying the relationship between them is the emphasis of this paper. These initiatives will undoubtedly affect how accurately GPP estimation is performed. Since there is an obvious relationship between optical parameters and chlorophyll-*a* concentration in Case I seawater [26,31–33], to achieve the above goal, we need to develop a parameterization scheme between the quanta-to-energy ratio and optical parameters (e.g., diffuse attenuation coefficient). Prior to that, we must appropriately distort and shorten the quanta-to-energy ratio calculation formula. In Section 2, the employed data are described, and a new parameter named the principal wavelength, is defined. In Section 3, the quantitative relationship between the vertical change in the quanta-to-energy ratio and chlorophyll-*a* concentration is discussed theoretically. In Section 4, the application is explored. Finally, in Section 5, the main conclusions are summarized.

2. Materials and Methods

2.1. Materials

The bio-optical observation was conducted in the Canada Joint Ocean-Ice Study (JOIS) science program onboard R/V CCGS Louis S. St-Laurent (an icebreaker of Canada) from 5 August to 14 September 2006. In total, 37 casts were finished during the cruise from 70–80° N and 160–120° W, spanning the Canada Basin (Figure 1A), and all stations are used in this paper to obtain the profiles of the quanta-to-energy ratio in the ocean.

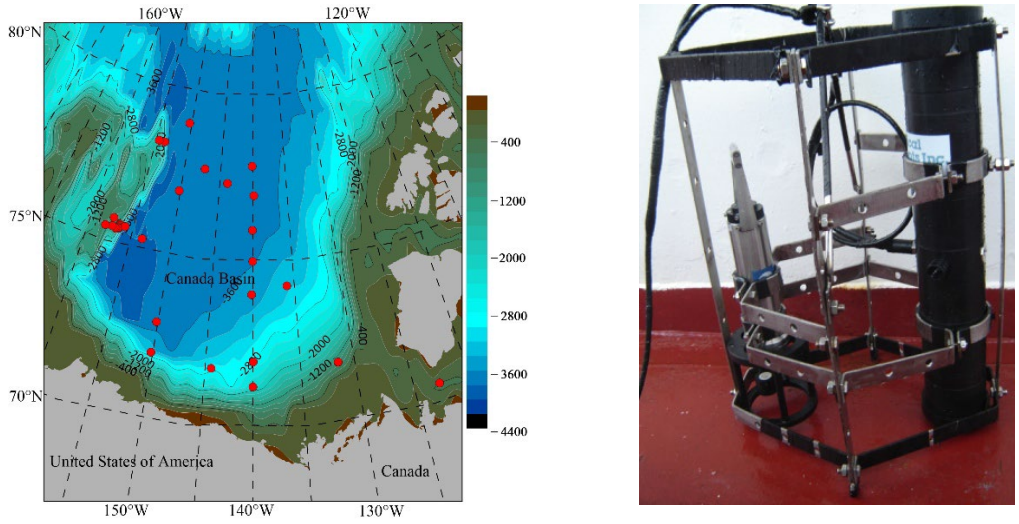

Figure 1. (**A**) Station map for the 2006 Canada Joint Ocean-Sea Study Science Program. The red dots represent the observation stations. (**B**) Optical observation instruments. The right black cylinder is the PRR800, and the left silver instrument is the MCTD.

The optical instruments PRR-800 and PRR-810 made by Biospherical Instruments Inc. (BSI, San Diego, CA, USA), were deployed to measure the underwater profiling of the downwelling irradiance (E_d) and surface downwelling irradiance (E_s), respectively, which collect signals simultaneously. Both instruments have 18 wavelengths (313, 380, 412, 443, 490, 510, 520, 532, 555, 565, 589, 625, 665, 683, 710, 765, 780, and 875 nm). Compact-CTD (MCTD) was used to collect the profile of chlorophyll-*a* concentration. PRR800 and MCTD were mounted on a frame and were lowered to approximately 100 m from the ship at the side facing the sun (Figure 1B).

2.2. Principal Wavelength

PAR has two types of measurement terms: the energy term (W, W m^{-2}) and the photon term (Q, μmol·m^{-2}·s^{-1}). The equations are as follows,

$$W = \int_{\lambda_1}^{\lambda_2} E(\lambda) d\lambda \tag{1}$$

$$Q = \frac{1}{A_v hc} \int_{\lambda_1}^{\lambda_2} E(\lambda) \lambda d\lambda \tag{2}$$

$$\frac{Q}{W} = \frac{1}{A_v hc} \frac{\int_{\lambda_1}^{\lambda_2} E(\lambda) \lambda d\lambda}{\int_{\lambda_1}^{\lambda_2} E(\lambda) d\lambda} = \frac{1}{A_v hc} \lambda_p \tag{3}$$

$$\lambda_p = \frac{\int_{\lambda_1}^{\lambda_2} E(\lambda)\lambda d\lambda}{\int_{\lambda_1}^{\lambda_2} E(\lambda) d\lambda} = \int_{\lambda_1}^{\lambda_1} \frac{E(\lambda)}{W}\lambda d\lambda \quad (4)$$

where Planck's constant $h = 6.6255 \times 10^{-34}$ W s^2, the velocity of light in vacuum $c = 2.9979 \times 10^{17}$ nm s^{-1}, and the Avogadro constant $A_v = 6.02 \times 10^{23}$ mol^{-1}. λ_1 and λ_2 are the lower and upper limits of the wavelength region under consideration, and generally correspond to 400 nm and 700 nm, respectively.

In Equation (3), Q/W may be reduced to the product of a constant and a variable with the dimension of wavelength. For monochromatic radiation, Q/W is a straightforward function of wavelength and does not rely on depth [28]. In Equation (4), $E_d(\lambda)/W$ is the ratio between the solar irradiance at wavelength λ and the integral of the solar irradiance from wavelength λ_1 to λ_2. We postulate that once the original solar spectrum passes through two hypothesized attenuation particles A and B in Figure 2, the principal wavelength corresponding to the solar spectrum is altered. When shortwave radiation is attenuated by attenuation particle A, it will increase the λ_p of incoming solar radiation. If a particle attenuates longwave radiation, as particle B presents an attenuation characteristic in Figure 2, the value of the λ_p on the wavelength axis will decrease. λ_p fluctuates when the spectral distribution of the irradiance varies. Here, λ_p is named the principal wavelength because of its property of having the dimension of wavelength.

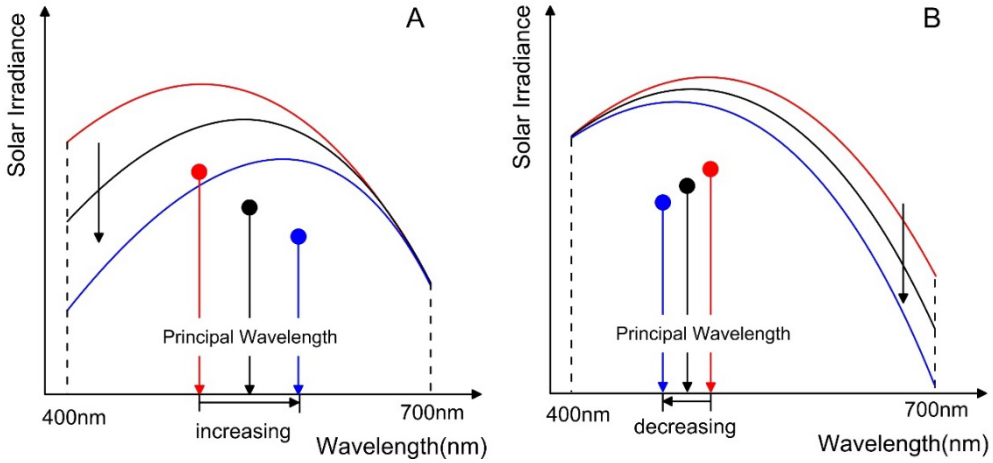

Figure 2. Sketches for the change in the principal wavelength. The original solar spectrum is shown by the red line. The solar spectrum changes after passing through two types of attenuation particles, (**A**) and (**B**), and becomes the black and blue lines depicting the entering solar spectrum. The "weight center" of the red, black, and blue lines is represented by the red, black, and blue points, respectively. The value of the principal wavelength is determined by the placements of their "weight centers" on the wavelength axis.

The vertical profile of the principal wavelength will be the subject in Section 3, because the principal wavelength can be translated by a constant from the quanta-to-energy ratio and has a substantial physical meaning. In Section 4, the principal wavelength can be used to determine Q/W, which is then utilized to establish a link with the chlorophyll-*a* concentration.

3. Theoretical Analysis of λ_p

3.1. Exponential Function of λ_p

Equation (4) can be simplified as,

$$\int (\lambda - \lambda_p(z)) E_d(z, \lambda) d\lambda = 0 \quad (5)$$

where $E_d\ (z,\ \lambda)$ is the downwelling irradiance under seawater and the integral range from 400 to 700 nm is ignored. Taking the derivation on both sides of Equation (5),

$$\frac{d\int(\lambda-\lambda_p(z))E_d(z,\lambda)d\lambda}{dz}=0 \tag{6}$$

where only λ_p and $E_d\ (z,\ \lambda)$ are functions of the depth. Simplifying Equation (6), we have

$$\frac{d\lambda_p(z)}{dz}-\lambda_p K_d(z)=\frac{1}{\int E_d(z,\lambda)d\lambda}\frac{d\int\lambda E_d(z,\lambda)d\lambda}{dz} \tag{7}$$

where $K_d(z,\lambda)$ is the attenuation coefficient of the photosynthetically radiant flux density (denoted by W), and its definitional expression is as follows:

$$K_d(z)=-\frac{1}{\int E_d(z,\lambda)d\lambda}\frac{d\int E_d(z,\lambda)d\lambda}{dz}=-\frac{1}{W(z)}\frac{dW(z)}{dz} \tag{8}$$

Here, we introduce another parameter similar to $K_d(z)$, denoted by $K_q(z)$:

$$K_q(z)=-\frac{1}{\int\lambda E_d(z,\lambda)d\lambda}\frac{d\int\lambda E_d(z,\lambda)d\lambda}{dz} \tag{9}$$

Substituting into the definition of Q, which is $Q(z)=\frac{1}{A_v hc}\int_{\lambda_1}^{\lambda_2}E(\lambda)\lambda d\lambda$,

$$K_q(z)=-\frac{1}{Q(z)}\frac{dQ(z)}{dz} \tag{10}$$

Similar to the $K_d(z)$ property, $K_q(z)$ quantifies the attenuation characteristic of the photo number. Using Equation (6) to replace Equation (7), we have

$$\frac{d\lambda_p}{dz}-\lambda_p K_d=-\lambda_p K_q \tag{11}$$

Its solution to the simplest differential equation is as follows:

$$\lambda_p(H)=\lambda_{p0}\exp\left[-\int_0^H(K_q(z)-K_d(z))dz\right] \tag{12}$$

Equation (12) demonstrates that λ_p has been attenuated following an exponential function. In Case I seawater, Chlorophyll-*a* has a great influence on the downwelling irradiance. The diffuse attenuation coefficient for the dowelling irradiance,K_d, is an important indicator in assessing the feedback of the phytoplankton biomass on the physical property of seawater [26]. There is an exponential empirical relationship between K_d and the chlorophyll-*a* concentration. The profiles of λ_p were calculated using the downwelling irradiance profile data observed in the Canada Basin in 2006, as shown in Figure 3.

The variation characteristics of λ_p are summarized as follows. (1). λ_p rapidly decreases in the upper 10 m and after exceeding 10, it is essentially stable. The profile of λ_p resembles that of an exponential function; (2). At 70 m, λ_p appears to have a regional characteristic. As indicated in Figure 3, λ_p in Canada Basin coastal water is chiefly highest, owing to runoff from the Mackenzie River, and lower in the west, where Pacific inflow pours into a depth from 30 to 60 m. The smallest value is found northeast of the Canada Basin, which is permanently covered in sea ice. (3). λ_p in Case I seawater is chiefly influenced by chlorophyll-*a*. The principal wavelength has already increased in seawater with high chlorophyll-*a* concentrations, such as the Pacific inflow east of the Canada Basin, which is intimately associated with the absorption spectrum of chlorophyll-*a*.

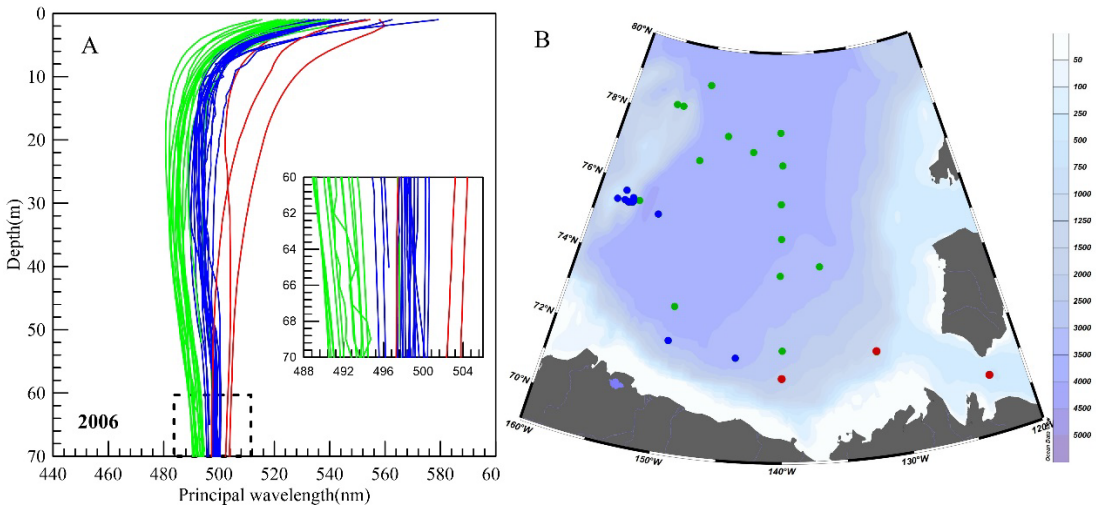

Figure 3. (**A**) The profiles of the principal wavelength recorded in the Canada Basin. The stations and accompanying profiles in (B) are indicated with red, blue, and green dots according to the classification of K_d (coastal type, inflow-influence type, and basin type). The subgraph in (**A**) enlarges the profiles of the principal wavelength at depths of 60–70 m.

3.2. The Deviation of the λ_p

The principal wavelength alone cannot reveal changes in the solar spectrum. Alternatively, it makes sense only when compared to a reference value. As a result, we must comprehend the deviation of the principal wavelength. The following is a hypothetical test: The light with a principal wavelength of $\lambda(z)$ becomes λ_0 as it travels through a pure seawater layer with a depth of dz. The principal wavelength becomes λ_1 when it passes through the seawater layer with a chlorophyll-*a* concentration of C ug/l. We have, according to Equation (12),

$$\lambda_0 = \lambda(z)\exp\left[-\left(K_q^0 - K_d^0\right)dz\right] \tag{13}$$

$$\lambda_1 = \lambda(z)\exp\left[-\left(K_q^1 - K_d^1\right)dz\right] \tag{14}$$

where superscripts "0" and "1" denote that solar radiation enters pure seawater and seawater with chlorophyll-*a*, respectively. As a result, the deviation of the principal wavelength is defined as follows:

$$\frac{\lambda_1}{\lambda_0} = \exp\left\{\left[-\left(K_q^1 - K_q^0\right) - \left(K_d^1 - K_d^0\right)\right]dz\right\} \tag{15}$$

Because dz is small enough to simplify Equation (15), e. g., K_d is

$$K_d = -\frac{1}{\int E_d d\lambda}\frac{d\int E_d d\lambda}{dz} = \frac{\int K_d E_d d\lambda}{\int E_d d\lambda} \tag{16}$$

and

$$K_q = -\frac{1}{\int \lambda E_d d\lambda}\frac{d\int \lambda E_d d\lambda}{dz} = \frac{\int \lambda K_d E_d d\lambda}{\int \lambda E_d d\lambda} \tag{17}$$

Therefore, $\left(K_q^1 - K_q^0\right)$ in Equation (15) can be simplified as follows:

$$K_q^1 - K_q^0 = \frac{\int \lambda\left(K_d^1 - K_d^0\right)E_d d\lambda}{\int \lambda E_d d\lambda} = \frac{\int \lambda \Delta K_d E_d d\lambda}{\int \lambda E_d d\lambda} \tag{18}$$

where ΔK_d is regarded as a non-water diffuse attenuation coefficient. Similarly,

$$K_d^1 - K_d^0 = \frac{\int (K_d^1 - K_d^0) E_d d\lambda}{\int E_d d\lambda} = \frac{\int \Delta K_d E_d d\lambda}{\int E_d d\lambda} \tag{19}$$

Equation (15) can be simplified by Equations (18) and (19):

$$\frac{\lambda_1}{\lambda_0} = \exp\left[-\left(\frac{\int \lambda \Delta K_d E_d d\lambda}{\int \lambda E_d d\lambda} - \frac{\int \Delta K_d E_d d\lambda}{\int E_d d\lambda}\right) dz\right] \tag{20}$$

Arranging Equation (19) is to take

$$\frac{d \ln \lambda_p}{dz} = -\left(\frac{\int \lambda \Delta K_d E_d d\lambda}{\int \lambda E_d d\lambda} - \frac{\int \Delta K_d E_d d\lambda}{\int E_d d\lambda}\right), \; d \ln \lambda_p = \ln \lambda_1 - \ln \lambda_0 \tag{21}$$

In Case I seawater, as λ_1 is greater than λ_0, the right of Equation (21) is greater than 0. It is concluded that $\left(\frac{\int \lambda \Delta K_d E_d d\lambda}{\int \lambda E_d d\lambda} - \frac{\int \Delta K_d E_d d\lambda}{\int E_d d\lambda}\right)$ is less than 0. Equation (21) represents the link between the real principal wavelength and the ideal principal wavelength of pure seawater.

Here, we introduce the spectral model of the diffuse attenuation coefficient, $\Delta K_d(\lambda) = a(\lambda) \Delta K_d(490)$. Thus, Equation (21) can be simplified as

$$\frac{d \ln \lambda_p}{dz} = -\left(\frac{\int \lambda \Delta K_d E_d d\lambda}{\int \lambda E_d d\lambda} - \frac{\int \Delta K_d E_d d\lambda}{\int E_d d\lambda}\right) = -\Delta K_d(490) \times \varepsilon \tag{22}$$

$$\varepsilon = \left(\frac{\int \lambda a(\lambda) E_d d\lambda}{\int \lambda E_d d\lambda} - \frac{\int a(\lambda) E_d d\lambda}{\int E_d d\lambda}\right) \tag{23}$$

The variable ε is solely related to the light field in seawater since the $a(\lambda)$ in Case I seawater is obtained and included as a constant at a given wavelength in Table 1. As indicated in Figure 4, the 37 profilers of ε from Figure 3 have been collected. The average value may be used as a constant because the variation between the 37 profiles is negligible. The absolute mean profile of ε demonstrates a continuous decreasing feature, indicating that the impact of chlorophyll-*a* on the deviation of λ_p decreases with depth, as shown by Equation (22). At the sea surface, the deviation of the same chlorophyll-*a* content is approximately 6 times greater than that at 70 m.

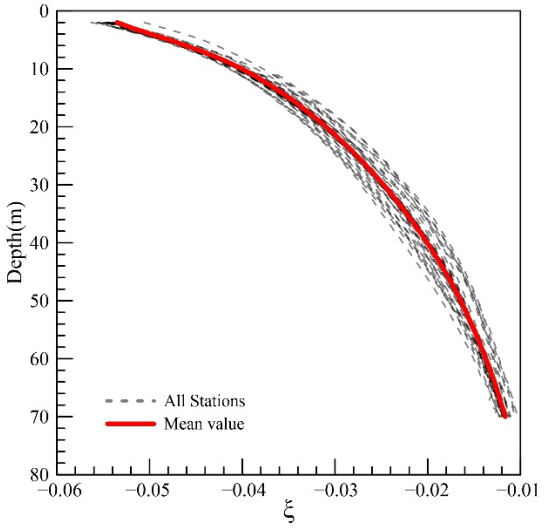

Figure 4. The 37 profiles and mean profile denoted by the red line for ε observed in the identical sites in Figure 3.

Table 1. The value $a(\lambda)$ at selected wavebands deduced from [34] and [26] by spline interpolation method.

λ/nm	$a(\lambda)$
412	1.7500
443	1.4360
490	1.0000
510	0.8310
520	0.7578
532	0.6804
555	0.5647
565	0.5289
589	0.4840
625	0.5659
665	0.7205
683	0.6000

The deviation of λ_p is dependent on the diffuse attenuation coefficient at 490 nm and the variable ε, as shown in Equation (22). The deviation can only be attributed to the former because of the constant characteristic of ε. The deviation of the principal wavelength exhibits a quasi-linear relationship with the non-water diffuse attenuation coefficient at 490 nm.

3.3. The Semi-Empirical Formula between λ_p and Chlorophyll-a Concentration

In reference [33] built a semi-empirical relationship between the diffuse attenuation coefficient at 490 nm and chlorophyll-*a* in Case I seawater as follows:

$$K_d(490) - K_w(490) = \chi(490) Chl^{e(490)} \tag{24}$$

where $K_d(490)$ is the observed diffuse attenuation coefficient. $K_w(490)$ is the diffuse attenuation coefficient of pure seawater and is approximated as the sum of the absorption and backscattering coefficients of optically pure seawater.

The deviation of λ_p is associated with the upper total attenuation matter concentration. Therefore, similar to Equation (24), we built an expression according to Equation (22) as follows:

$$\ln \lambda_p(z) - \ln \lambda_{p0}(z) = A \times \left(\sum_0^z Chl(h) \Delta h \right)^B \tag{25}$$

where $\lambda_p(z)$ is the observed value (the integral range is 400~700 nm), and the ideal λ_{p0} is the simulated value in pure seawater at a depth of z. Based on the identical surface radiation spectra, the ideal λ_p is calculated from pure water at the depth of z. From 0 to z, $\sum_0^z Chl(h)\Delta h$ is the integral of the chlorophyll-*a* concentration. In Figure 3a, the chlorophyll-*a* concentration is measured synchronously using a fluorescent probe mounted on ALEC MCTD. According to the data in Figure 3a, the regression coefficients A and B are 0.0278 and 0.4733, respectively. The fitting results are depicted in Figure 5a.

In addition, according to Equation (23), the profile of the deviation is closely related to the variable ε. Therefore, Equation (25) is modified simply as follows,

$$\left[\ln \lambda_p(z) - \ln \lambda_{p0}(z) \right] \times \frac{1}{\varepsilon_0} = A \times \left(\sum_0^z Chl(h) \Delta h \right)^B \tag{26}$$

where ε_0 is the value of ε below the sea surface.

According to Equation (26), the regression coefficients (A and B) are obtained and equal to 0.545 and 0.4771, respectively, in Figure 5b. There is little difference in the determination coefficient obtained by Equations (25) and (26). The determination coefficients obtained by the two fitting equations are generally consistent, 0.843 and 0.838, respectively.

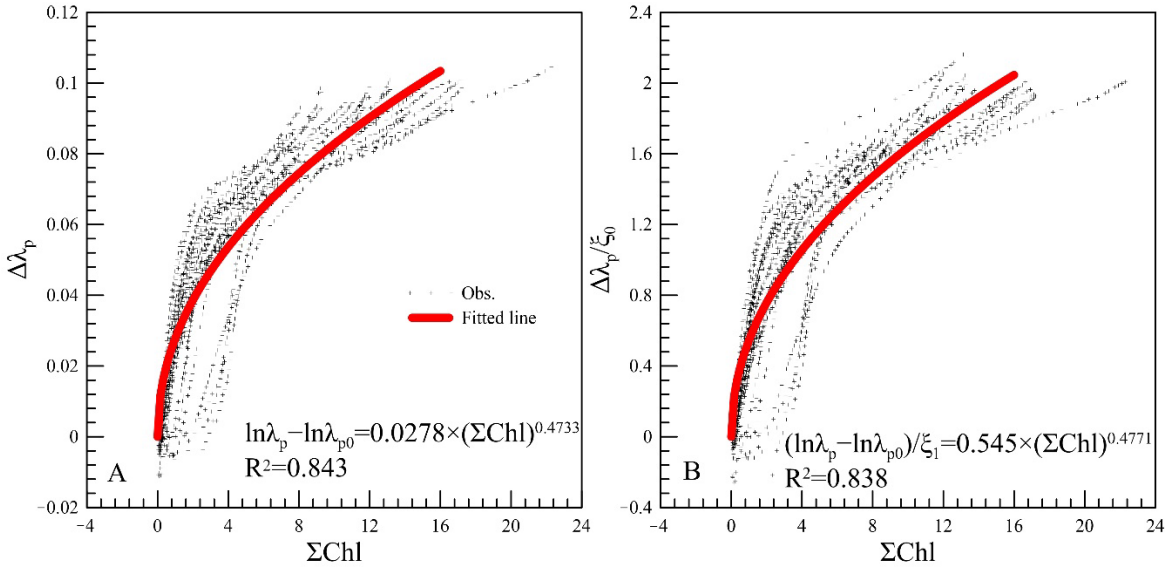

Figure 5. The fitting relationship between the deviation of λ_p (relative to the ideal λ_{p0} in pure seawater) and the integrated chlorophyll-*a* concentration according to Equation (25) (**A**) and Equation (26) (**B**), respectively.

3.4. The Ideal Profile of λ_{p0} for Pure Seawater

To obtain the profile of λ_{p0}, we extrapolate the spectral distribution of the downwelling irradiance at the sea surface using 37 observation data in Figure 3. The underwater radiation spectrum is reproduced in the range from 0 to 70 m by introducing the diffusion attenuation coefficient of pure seawater. As illustrated in Figure 6, the profiles of λ_{p0} may be calculated using the simulated radiation spectrum data.

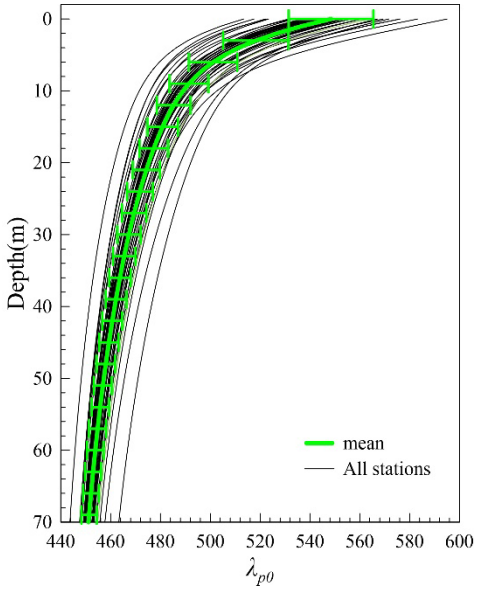

Figure 6. The profiles of λ_{p0} in the 37 observation data acquired from the simulation radiation spectrum based on $E_d(0^-)$. The green line denotes the mean value and error bar of λ_{p0}.

Since the long wave (>500 nm) has been quickly absorbed in the surface seawater, the solar radiation that reaches the deep layer is primarily concentrated in the range from 440 to 460 nm. This is characterized by a rapid decrease in the surface layer and concentration in the deep layer at the principal wavelength. Because the solar zenith angle, cloud cover, and atmospheric conditions vary over the observation period, the standard deviation of

λ_{p0} at the sea surface exceeds 17 nm. The standard deviation gradually lowers as depth increases, until it is barely 3 nm at 70 m. With increasing depth, λ_{p0} decays exponentially on average. According to Equation (12), the fitting relationship between λ_{p0} and depth (z) is as follows:

$$\lambda_{p0}(z) = \lambda_p(0^-)\left\{0.12 \times e^{-0.1642z} + 0.88 \times e^{-0.00098z}\right\} \quad (27)$$

We can obtain the parameterized formula of the principal wavelength in Case I seawater with chlorophyll-*a* concentration using Equations (25) and (27), as shown below.

$$\ln \lambda_p(z) = 0.0278 \times \left(\sum_0^z Chl(h)\Delta h\right)^{0.4733} + \ln\{\lambda_p(0^-)\left\{0.12 \times e^{-0.1642z} + 0.88 \times e^{-0.00098z}\right\} \quad (28)$$

4. Discussion

We developed a parameterized formula for the quanta-to-energy ratio of photosynthetically active radiation in Case I seawater based on the foregoing correlations, as follows:

$$\frac{Q}{W} = \frac{\lambda_p(0^-)}{A_v hc}\left(0.12 \times e^{-0.1642z} + 0.88 \times e^{-0.00098z}\right) \exp\left[0.0278 \times \left(\sum_0^z Chl(h)\Delta h\right)^{0.4733}\right] \quad (29)$$

The Q/W profiles at 37 stations are obtained using Equation (29). Compared with the observed values, the average relative error is calculated using the observed data, as illustrated in Figure 7. The Q/W calculated by the parameterization formula is found to be somewhat larger than the observed value. The relative inaccuracy is lowest at the surface layer and gradually increases with depth. The relative inaccuracy in the range from 0 to 70 m must not exceed 10%.

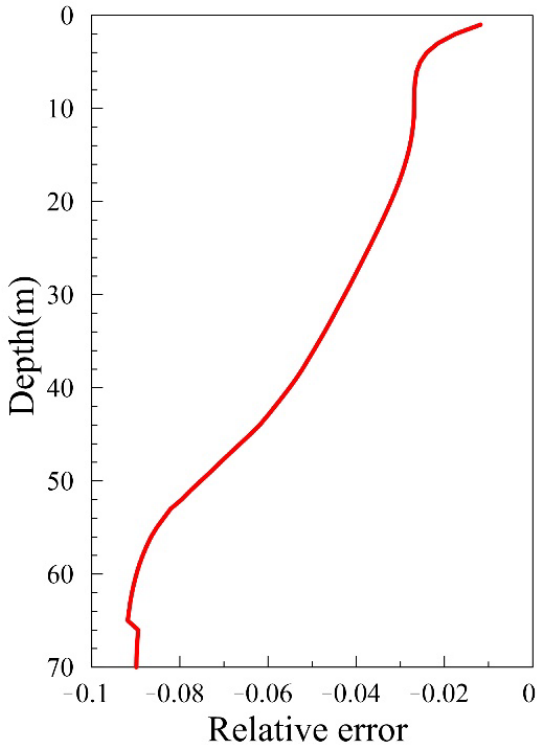

Figure 7. The relative inaccuracy profile of Q/W in the Canada Basin.

The principal wavelength may replace the quanta-to-energy ratio in converting to Q from solar radiation, and it is a new proposed physical parameter that is a weighted mean of the solar radiation spectrum. The anomaly of the principal wavelength on the surface is small, measuring only a few nanometers. However, in seawater, its variance might approach more than a hundred nanometers. Additionally, the principal wavelength varies significantly by region. In contrast to PAR, which reflects the residual intensity of

arriving solar radiation, the principal wavelength represents the remaining solar radiation spectrum. Both thus lead to a comprehensive understanding of the fundamental properties of arriving solar radiation.

The principal wavelength is connected not only to the chlorophyll-*a* concentration at a certain level but also to the matter in the entire column above the measuring level, allowing us to investigate the influence of the attenuation matter and its vertical distribution on the transmitting radiation. In addition, the principal wavelength is sensitive to reflect the regional difference of arriving irradiance influenced by the matter. Thus, it is possible to use the principal wavelength to identify or classify the regional feature of seawater.

5. Conclusions

The formula of the quanta-to-energy ratio of photosynthetically active radiation is properly distorted and simplified in this study into the product of a constant and principal wavelength, which is the dimension of wavelength. The theoretical relationship of the principal wavelength with other factors, such as the attenuation coefficient and chlorophyll-*a* concentration, has been explored using solar radiative transfer theory. The following are the outcomes: (i) the function of the principal wavelength with depth has been developed, demonstrating the exponential decrease in the principal wavelength in seawater; (ii) the deviation of the principal wavelength is defined in theory as the ratio of the measured principal wavelength to the simulated value in pure seawater in the same solar radiation at the sea surface. The deviation of the principal wavelength has a quasi-linear relationship with the non-water diffuse attenuation coefficient at 490 nm. (iii) An association is established between the principal wavelength and chlorophyll-*a* concentration. The obtained determination coefficient in Case I seawater is more than 80%; (iv) the principal wavelength at the sea surface may be used to derive the profile of the principal wavelength for pure seawater. According to the preceding derivation, the parameterized formula is appropriate for estimating the global distribution of the ratio since it is simply connected to the chlorophyll-*a* profile and surface principal wavelength. However, owing to the unique bio-optical features of Arctic seawater [26,35,36], such as pronounced pigment packaging, additional investigation is required in terms of the bio-optical relationship and pure seawater profile of the principal wavelength.

The quanta-to-energy ratio can be replaced by the principal wavelength, which has a more profound physical meaning. Back to our issue, we may use Figure 8 to illustrate the relationship between the quanta-to-energy ratio and the chlorophyll-a in Case I seawater. Using the profile in the principal wavelength of pure water as a baseline, the principal wavelength of arriving solar radiation is changed dramatically with the increase in depth, and its amplitude is governed by the total chlorophyll-*a* concentration above the measuring level. The difference can be expressed by Equation (25). That is, the higher the integral of the chlorophyll-a concentration in the upper layer, the greater the shift in the arriving principal wavelength, which explains the ability of the arriving principal wavelength displaying the difference in bio-optical properties of seawater over the Beaufort Sea in Figure 3.

The description of the variation of the principal wavelength profile in Case I seawater is essentially compatible with the findings reported by Reinart et al. [28]. The profiles of the principal wavelength in Case II and III seawater provided by Reinart et al. [28] show a considerable difference from that in Case I seawater. Some formulas developed in this paper only apply to the Case I seawater. However, certain formulations, such as Equations (12) and (21), can explain the variation in the profile of Case II and III seawater. They set the groundwork for future research on the shift in the principal wavelength in Case II and III seawater.

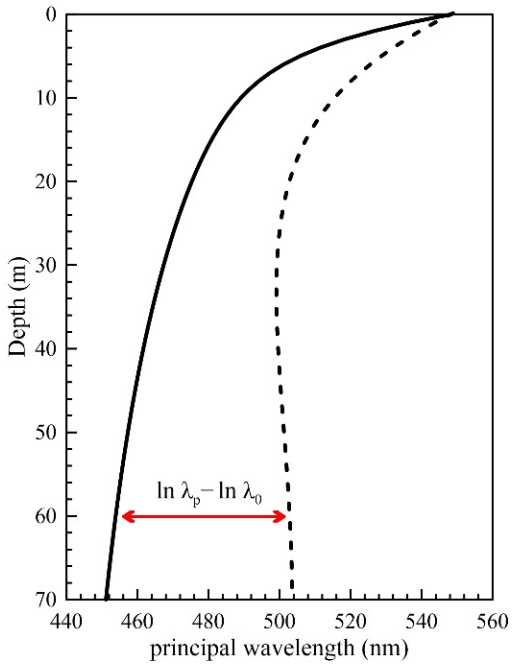

Figure 8. Schematic diagram of the relationship between the principal wavelength and chlorophyll-a concentration. The black line is the average principal wavelength of pure seawater (λ_{p0}), and the dotted line represents the schematic profile of the principal wavelength in Case I seawater. The difference between the two at 60 m is displayed.

Author Contributions: Conceptualization, W.W. and J.Z. (Jinping Zhao); methodology, W.W. and J.Z. (Jinping Zhao); software, J.Z. (Jianhua Zheng); validation, W.W., J.Z. (Jinping Zhao); formal analysis, W.W.; investigation, W.W. and J.Z. (Jinping Zhao); resources, J.Z. (Jianhua Zheng); data curation, W.W.; writing—original draft preparation, W.W.; writing—review and editing, J.Z. (Jianhua Zheng) and C.J.; visualization, W.W.; supervision, C.J.; project administration, C.J.; funding acquisition, C.J. All authors have read and agreed to the published version of the manuscript.

Funding: This research was funded by Global Change and Air-sea Interaction II (No. GASI-01-SIND-STwin and GASI-01-NPAC-STsum), the National Natural Science Foundation of China (42130406) and the Scientific Research Foundation of the Third Institute of Oceanography, MNR, China (No. 2016023).

Institutional Review Board Statement: Not applicable.

Informed Consent Statement: Not applicable.

Data Availability Statement: Not applicable.

Acknowledgments: Thank Jiuxin Shi and Yutian Jiao for their on-site observation and the R/V CCGS Louis S. St-Laurent crew for their help. We would like to thank the reviewers who have provided suggestions for improving the manuscript of this article.

Conflicts of Interest: The authors declare no conflict of interest.

References

1. Zhao, J.; Wang, W.; Cooper, L. Calculation of Photosynthetically Available Radiation Using Multispectral Data in the Arctic. *Chin. J. Polar Res.* **2010**, *22*, 91–103. [CrossRef]
2. Alados, I.; Foyo-Moreno, I.; Alados-Arboledas, L. Photosynthetically Active Radiation: Measurements and Modelling. *Agric. For. Meteorol.* **1996**, *78*, 121–131. [CrossRef]
3. Frouin, R.; Lingner, D.W.; Gautier, C.; Baker, K.S.; Smith, R.C. A Simple Analytical Formula to Compute Clear Sky Total and Photosynthetically Available Solar Irradiance at the Ocean Surface. *J. Geophys. Res. Ocean.* **1989**, *94*, 9731–9742. [CrossRef]
4. Emmanuel, D.; Phillipe, D.; Malik, C. Radiative Transfer Code: Application to the Calculation of PAR. *J. Earth Syst. Sci.* **2000**, *109*, 407–413. [CrossRef]

5. Akitsu, T.K.; Nasahara, K.N.; Ijima, O.; Hirose, Y.; Ide, R.; Takagi, K.; Kume, A. The Variability and Seasonality in the Ratio of Photosynthetically Active Radiation to Solar Radiation: A Simple Empirical Model of the Ratio. *Int. J. Appl. Earth Obs. Geoinf.* **2022**, *108*, 102724. [CrossRef]
6. Zhou, H.; Yue, X.; Lei, Y.; Zhang, T.; Tian, C.; Ma, Y.; Cao, Y. Responses of Gross Primary Productivity to Diffuse Radiation at Global FLUXNET Sites. *Atmos. Environ.* **2021**, *244*, 117905. [CrossRef]
7. Huang, G.; Li, X.; Lu, N.; Wang, X.; He, T. A General Parameterization Scheme for the Estimation of Incident Photosynthetically Active Radiation under Cloudy Skies. *IEEE Trans. Geosci. Remote Sens.* **2020**, *58*, 6255–6265. [CrossRef]
8. Mercado, L.M.; Bellouin, N.; Sitch, S.; Boucher, O.; Huntingford, C.; Wild, M.; Cox, P.M. Impact of Changes in Diffuse Radiation on the Global Land Carbon Sink. *Nature* **2009**, *458*, 1014–1017. [CrossRef]
9. Ren, X.; He, H.; Zhang, L.; Yu, G. Global Radiation, Photosynthetically Active Radiation, and the Diffuse Component Dataset of China, 1981–2010. *Earth Syst. Sci. Data* **2018**, *10*, 1217–1226. [CrossRef]
10. Alados, I.; Olmo, F.J.; Foyo-Moreno, I.; Alados-Arboledas, L. Estimation of Photosynthetically Active Radiation under Cloudy Conditions. *Agric. For. Meteorol.* **2000**, *102*, 39–50. [CrossRef]
11. Sasai, T.; Ichii, K.; Yamaguchi, Y.; Nemani, R. Simulating Terrestrial Carbon Fluxes Using the New Biosphere Model "Biosphere Model Integrating Eco-Physiological and Mechanistic Approaches Using Satellite Data" (BEAMS). *J. Geophys. Res. Biogeosci.* **2005**, 110. [CrossRef]
12. Zhao, M.; Running, S.W.; Nemani, R.R. Sensitivity of Moderate Resolution Imaging Spectroradiometer (MODIS) Terrestrial Primary Production to the Accuracy of Meteorological Reanalyses. *J. Geophys. Res. Biogeosci.* **2006**, 111. [CrossRef]
13. Akitsu, T.; Kume, A.; Hirose, Y.; Ijima, O.; Nasahara, K.N. On the Stability of Radiometric Ratios of Photosynthetically Active Radiation to Global Solar Radiation in Tsukuba, Japan. *Agric. For. Meteorol.* **2015**, *209–210*, 59–68. [CrossRef]
14. González, J.A.; Calbó, J. Modelled and Measured Ratio of PAR to Global Radiation under Cloudless Skies. *Agric. For. Meteorol.* **2002**, *110*, 319–325. [CrossRef]
15. Moon, P. Proposed Standard Solar-Radiation Curves for Engineering Use. *J. Franklin Inst.* **1940**, *230*, 583–617. [CrossRef]
16. Mizoguchi, Y.; Yasuda, Y.; Ohtani, Y.; Watanabe, T.; Kominami, Y.; Yamanoi, K. A Practical Model to Estimate Photosynthetically Active Radiation Using General Meteorological Elements in a Temperate Humid Area and Comparison among Models. *Theor. Appl. Climatol.* **2014**, *115*, 583–589. [CrossRef]
17. Foyo-Moreno, I.; Alados, I.; Alados-Arboledas, L. A New Conventional Regression Model to Estimate Hourly Photosynthetic Photon Flux Density under All Sky Conditions. *Int. J. Climatol.* **2017**, *37*, 1067–1075. [CrossRef]
18. Aguiar, L.J.G.; Fischer, G.R.; Ladle, R.J.; Malhado, A.C.M.; Justino, F.B.; Aguiar, R.G.; da Costa, J.M.N. Modeling the Photosynthetically Active Radiation in South West Amazonia under All Sky Conditions. *Theor. Appl. Climatol.* **2012**, *108*, 631–640. [CrossRef]
19. Meek, D.W.; Hatfield, J.L.; Howell, T.A.; Idso, S.B.; Reginato, R.J. Generalized Relationship between Photosynthetically Active Radiation and Solar Radiation. *Agron. J.* **1984**, *76*, 939–945. [CrossRef]
20. Ge, S.; Smith, R.G.; Jacovides, C.P.; Kramer, M.G.; Carruthers, R.I. Dynamics of Photosynthetic Photon Flux Density (PPFD) and Estimates in Coastal Northern California. *Theor. Appl. Climatol.* **2011**, *105*, 107–118. [CrossRef]
21. Udo, S.O.; Aro, T.O. Global PAR Related to Global Solar Radiation for Central Nigeria. *Agric. For. Meteorol.* **1999**, *97*, 21–31. [CrossRef]
22. Li, R.; Zhao, L.; Ding, Y.; Wang, S.; Ji, G.; Xiao, Y.; Liu, G.; Sun, L. Monthly Ratios of PAR to Global Solar Radiation Measured at Northern Tibetan Plateau, China. *Sol. Energy* **2010**, *84*, 964–973. [CrossRef]
23. McCree, K.J. Test of current definitions of photosynthetically active radiation against leaf photosynthesis data. *Agric. Meteorol.* **1972**, *10*, 443–453. [CrossRef]
24. Morel, A.; Smith, R.C. Relation between Total Quanta and Total Energy for Aquatic Photosynthesis. *Limnol. Oceanogr.* **1974**, *19*, 591–600. [CrossRef]
25. Zhao, J.; Wang, W.; Kang, S.H.; Yang, E.J.; Kim, T.W. Optical Properties in Waters around the Mendeleev Ridge Related to the Physical Features of Water Masses. *Deep. Sea Res. Part II Top. Stud. Oceanogr.* **2015**, *120*, 43–51. [CrossRef]
26. Wang, W.; Zhao, J. Variation of Diffuse Attenuation Coefficient of Downwelling Irradiance in the Arctic Ocean. *Acta Oceanol. Sin.* **2014**, *33*, 53–62. [CrossRef]
27. Chang, G.C.; Dickey, T.D. Coastal Ocean Optical Influences on Solar Transmission and Radiant Heating Rate. *J. Geophys. Res. Ocean.* **2004**, *109*, C01020. [CrossRef]
28. Reinart, A.; Arst, H.; Blanco-Sequeiros, A.; Herlevi, A. Relation between Underwater Irradiance and Quantum Irradiance in Dependence on Water Transparency at Different Depths in the Water Bodies. *J. Geophys. Res. Ocean.* **1998**, *103*, 7749–7752. [CrossRef]
29. Lavoie, D.; Denman, K.; Michel, C. Modeling Ice Algal Growth and Decline in a Seasonally Ice-Covered Region of the Arctic (Resolute Passage, Canadian Archipelago). *J. Geophys. Res. Ocean.* **2005**, *110*, 1–17. [CrossRef]
30. Dye, D.G. Spectral Composition and Quanta-to-Energy Ratio of Diffuse Photosynthetically Active Radiation under Diverse Cloud Conditions. *J. Geophys. Res. Atmos.* **2004**, *109*, 1–12. [CrossRef]
31. Lee, Z.P.; Du, K.P.; Arnone, R. A Model for the Diffuse Attenuation Coefficient of Downwelling Irradiance. *J. Geophys. Res. C Ocean.* **2005**, *110*, 1–10. [CrossRef]

32. Lee, Z.P.; Darecki, M.; Carder, K.L.; Davis, C.O.; Stramski, D.; Rhea, W.J. Diffuse Attenuation Coefficient of Downwelling Irradiance: An Evaluation of Remote Sensing Methods. *J. Geophys. Res. C Ocean.* **2005**, *110*, 1–9. [CrossRef]
33. Morel, A. Are the Empirical Relationships Describing the Bio-Optical Properties of Case 1 Waters Consistent and Internally Compatible? *J. Geophys. Res. Ocean.* **2009**, *114*, 1–15. [CrossRef]
34. Austin, R.W.; Petzold, T.J. Spectral Dependence of the Diffuse Attenuation Coefficient of Light in Ocean Waters. *Ocean. Optics. VII* **1984**, *489*, 1689–1699. [CrossRef]
35. Babin, M.; Arrigo, K.; Bélanger, S.; Forget, M.-H.; Frouin, R.; Hill, V.; Hirawake, T.; Matsuoka, A.; Mitchell, B.G.; Reynolds, R.A. *Ocean Colour Remote Sensing in Polar Seas*; International Ocean Colour Coordinating Group: Dartmouth, NS, Canada, 2015.
36. Cota, G.F.; Harrison, W.G.; Platt, T.; Sathyendranath, S.; Stuart, V. Bio-Optical Properties of the Labrador Sea. *J. Geophys. Res. Ocean.* **2003**, 108. [CrossRef]